島根大学地球資源環境学研究報告　22, 161～166 ページ（2003 年 12 月）
Geoscience Rept. Shimane Univ., 22, p.161～166（2003）

Article

Calculated X-ray powder diffraction patterns for synthetic piemontite on the join $Ca_2Al_3Si_3O_{12}(OH)$–$Ca_2Mn^{3+}{}_3Si_3O_{12}(OH)$

Mariko Nagashima* and Masahide Akasaka*

Abstract

X-ray powder diffraction patterns of $Ca_2Al_3Si_3O_{12}(OH)$–$Ca_2Mn^{3+}{}_3Si_3O_{12}(OH)$ series synthetic piemontites were simulated with the Rietan-2000 program to clarify the X-ray powder diffraction pattern of piemontite, using cell parameters, site occupancies and atomic positions refined by the X-ray RIETVELD method. The compositions of $Ca_2Al_{3-p}Mn^{3+}{}_pSi_3O_{12}(OH)$–piemontites used were p = 0.5, 0.75, 1.0 and 1.25. The d-values of the strongest line in the simulated powder patterns show a nonlinear variation comparable to nonlinear changes in unit-cell parameters. The calculated powder patterns are very useful for indexing the Miller indices to each reflection in X-ray powder diffraction patterns of natural piemontite, to avoid misindexing and miscalculation of the unit-cell parameters. By comparison with these simulated X-ray powder patterns, we can evaluate the effects of preferred orientation in measured X-ray powder diffraction patterns, which is important for X-ray powder crystal structure analysis.

Key words: piemontite, epidote group, synthesis, X-ray powder diffraction, XRD, powder pattern

Introduction

Piemontite, an epidote group mineral, is mainly composed of $Ca_2Al_3Si_3O_{12}(OH)$ (clinozoisite: Cz), $Ca_2Mn^{3+}{}_3Si_3O_{12}(OH)$ (piemontite: Pm) and $Ca_2Fe^{3+}{}_3Si_3O_{12}(OH)$ (pistacite: Ps) components. Crystal structures of natural piemontite have been investigated in terms of single crystal structure refinements (Dollase, 1969, 1971; Kvick et al., 1988; Ferraris et al., 1989; Bonazzi et al., 1990, 1992; Bonazzi and Menchetti, 1994, 1995; Langer et al., 2002; and others). However, because natural piemontites commonly contain not only Mn^{3+} but also Fe^{3+} in the octahedral sites and other larger cations such as Sr, Mn^{2+} and/or REE in the *A2* site, the unit-cell parameters and structural parameters of piemontite in the Cz–Pm join have been not determined by the study of natural piemontite. In fact, the unit-cell parameters of natural piemontites vary considerably from sample to sample. Thus, Anastasiou and Langer (1977) synthesized $Ca_2Al_{3-p}Mn^{3+}{}_pSi_3O_{12}(OH)$-piemontites at 1.5 GPa and 800°C, and studied the variation of unit-cell parameters caused by the substitution of Mn^{3+} for Al. They assigned indices to the diffraction peaks and calculated d-values, but crystal structure refinements of their synthetic piemontites were not carried out due to the very fine grained nature of their samples. Despite their single crystal structural refinement of some synthetic Cz–Pm piemontites, Langer et al. (2002) did not present simulated X-ray powder diffraction patterns.

In our study, we investigated the crystal structures of the Cz–Pm series piemontites synthesized at 350 MPa and 500 °C, to compare them to piemontites synthesized at higher pressures and temperatures by Anastasiou and Langer (1977) and Langer et al. (2002). In this paper, we report the calculated X-ray powder diffraction patterns of synthetic $Ca_2Al_{3-p}Mn^{3+}{}_pSi_3O_{12}(OH)$-piemontites with p = 0.5, 0.75, 1.0 and 1.25, by using refined structural parameters which are shown in Nagashima and Akasaka (in press).

*Department of Materials Creation and Circulation Technology, Interdisciplinary Graduate School of Science and Engineering, Shimane University

Experimental Methods

Oxide mixtures were used as starting materials for the piemontite syntheses. Each reagent-grade chemical was treated as follows: $CaCO_3$ and MnO_2 were heated at 110°C for 3 hours, Al_2O_3 was heated at 1100°C for 3 hours, and SiO_2 was heated at 1350°C until amorphous silica was transformed to cristobalite. Appropriate amounts of $CaCO_3$, Al_2O_3, MnO_2 and SiO_2 were mixed to produce compositions of $Ca_2Al_{3-q}Mn^{3+}{}_qSi_3O_{12.5}$, where q = 0.5, 0.75, 1.0 and 1.5. The mixtures were heated at 850°C in air for one hour to break down the carbonate. MnO_2 was also converted to Mn_2O_3 by this treatment. Complete decomposition of the carbonate and conversion of MnO_2 to Mn_2O_3 were confirmed by X-ray powder diffraction analysis of the heated starting materials.

The oxide mixture starting materials were sealed in $Ag_{90}Pd_{10}$ capsules with excess distilled water. An Mn_2O_3/MnO_2 oxygen buffer was used to produce fO_2 adequate to maintain manganese in the trivalent state. Our hydrothermal syntheses were carried out at P_{fluid} of 350 MPa and temperatures of 500°C, using standard cold-seal pressure vessels.

Run products were identified using X-ray powder diffractometry (Cu Kα radiation). Chemical compositions of the synthetic phases were analyzed using a JEOL JXA-8800M

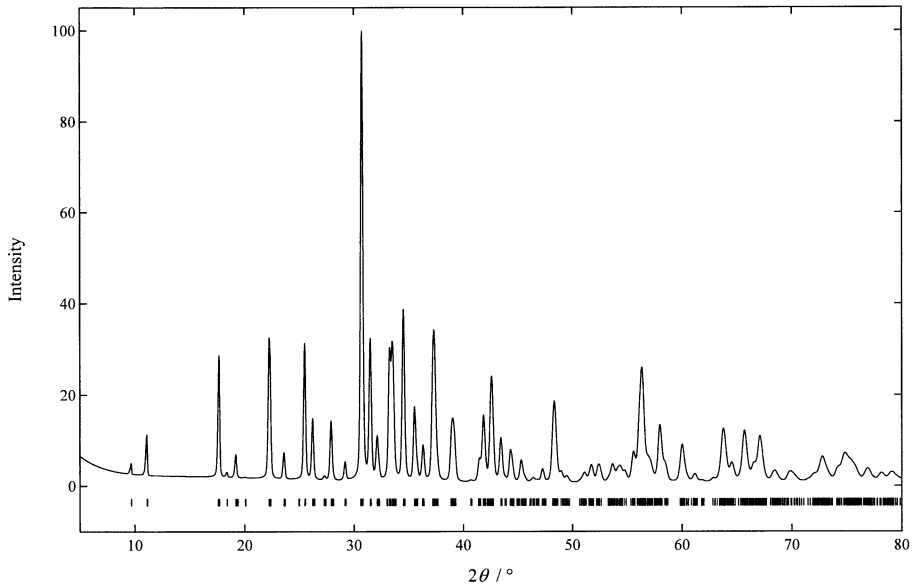

Fig. 1. The simulated pattern of p = 1.0 piemontite synthesized at 350 MPa and 500℃

electron probe micro analyzer operated at 15 kV, with beam current of 2.00×10^{-8} A and beam diameter of 1 μm. The oxidation state of Mn in synthetic piemontites was determined from relative intensities of Lα and L$_\beta$ X-ray emission peaks (Albee and Chodos, 1970; Kimura and Akasaka, 1999). Those intensities were measured with the JEOL JXA-8800M operating at 15 kV, using a TAP crystal (Kimura and Akasaka, 1999).

Grinding samples to a very small particle size is one of the most critical requirements for any structure study based on powder X-ray diffraction data (Bish and Reynolds, 1989; Post and Bish, 1989). To achieve this, samples were finely ground under alcohol in a hand agate mortar and pestle until particle sizes were less than 5 μm. Powdered samples were mounted in glass sample holders. Mounts for intensity profile collection were made by loading the powder from the front of the holder. Step-scan powder diffraction data were collected using a RIGAKU RINT automated X-ray powder diffractometer using a Bragg-Brentano goniometer equipped with incident- and diffracted-beam soller slits, 1° divergence and anti-scatter slits, a 0.15 mm receiving slit, and a curved graphite diffracted-beam monochrometer. The normal-focus Cu X-ray tube was operated at 35 kV and 25 mA. Profiles were taken between 10.00° and 150.00° 2θ at a step interval of 0.04° 2θ, using step counting times that accumulated around five thousand counts for the strongest peaks.

Crystal structures of synthetic piemontites were refined using the RIETAN-2000 program of Izumi and Ikeda (2000). The cell parameters determined using a unit-cell parameter refinement program in the RIGAKU RINT system were used as initial values. Peaks were defined using a 'Modified split pseudo-Voigt' function, which comprised the split pseudo-Voigt function of Toraya (1990) combined

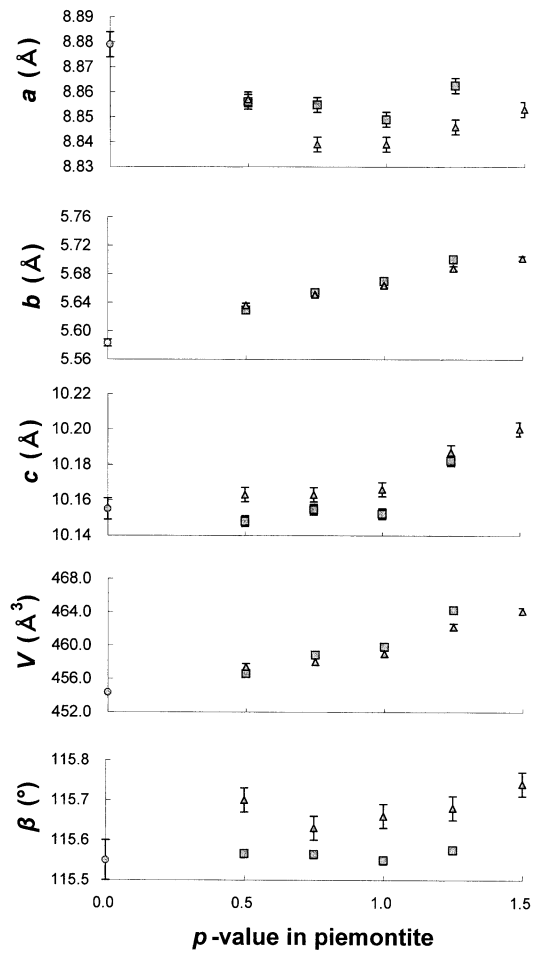

Fig. 2. Variations of unit-cell parameters as a function of p-value of piemontite. Error bars represent one standard deviation. Filled squares: unit-cell parameters of synthetic piemontites in this study; filled triangles: unit-cell parameters obtained by Anastasiou and Langer (1977); filled circle: the unit-cell parameter of clinozoisite obtained by Dollase (1968).

Table 1. Calculated powder X-ray diagram of synthetic piemontite crystallized from p = 0.5 starting material at 350 MPa and 500°C. All 2θ-values are given for CuKα

h	k	l	2θ	$d_{calc.}$	I/I_0	h	k	l	2θ	$d_{calc.}$	I/I_0	h	k	l	2θ	$d_{calc.}$	I/I_0
0	0	1	9.649	9.1588	1	-1	2	3	41.744	2.1620	4	1	0	5	56.087	1.6384	1
1	1	0	11.060	7.9929	5	-4	0	1	41.882	2.1552	11	-1	0	6	56.224	1.6347	10
-1	0	2	17.679	5.0126	24	-4	0	3	42.006	2.1491	3	-5	1	1	56.368	1.6309	12
0	1	1	18.489	4.7948	3	0	1	4	42.593	2.1209	1	4	2	0	56.432	1.6292	3
-1	1	1	19.304	4.5941	2	2	2	1	42.798	2.1111	17	-5	1	4	56.555	1.6260	1
2	0	0	22.226	3.9965	15	-2	2	3	42.920	2.1054	16	2	1	4	56.622	1.6242	2
-2	0	2	22.335	3.9772	13	0	2	3	43.713	2.0691	12	-4	2	4	56.630	1.6240	12
1	1	1	23.674	3.7551	7	-4	1	2	43.906	2.0604	1	1	2	4	56.678	1.6227	7
-2	1	1	25.575	3.4801	24	2	0	3	44.391	2.0390	6	2	3	1	56.879	1.6175	2
1	0	2	26.246	3.3927	10	-3	2	1	44.708	2.0253	3	3	2	2	57.141	1.6107	4
2	0	1	27.917	3.1932	12	-3	2	2	44.752	2.0234	2	0	3	3	57.625	1.5983	4
-2	0	3	28.094	3.1736	2	4	0	0	45.347	1.9982	6	-4	0	6	58.082	1.5868	14
0	0	3	29.228	3.0529	2	-1	0	5	45.766	1.9809	1	-3	3	1	58.442	1.5779	8
-3	0	1	30.618	2.9174	1	-3	0	5	46.477	1.9523	2	1	1	5	58.637	1.5731	6
-3	0	2	30.679	2.9118	15	2	1	3	47.381	1.9171	1	5	1	0	60.121	1.5378	2
-1	1	3	30.848	2.8963	100	2	2	2	48.442	1.8776	8	4	1	2	60.197	1.5360	6
0	2	0	31.775	2.8138	34	1	1	4	48.567	1.8730	5	-3	3	3	60.397	1.5314	4
2	1	1	32.204	2.7773	12	-2	2	4	48.608	1.8715	15	-4	2	5	61.407	1.5086	2
-2	1	3	32.359	2.7643	2	-1	2	4	48.619	1.8712	5	-5	2	2	62.041	1.4947	1
0	2	1	33.282	2.6898	1	-1	1	5	48.691	1.8685	4	-5	2	1	63.804	1.4576	1
0	1	3	33.362	2.6835	27	3	1	2	49.082	1.8546	3	-6	0	4	63.886	1.4559	5
3	0	0	33.610	2.6643	15	1	3	0	49.894	1.8263	1	3	0	4	63.967	1.4543	2
1	2	0	33.742	2.6542	20	0	2	4	51.407	1.7760	2	-5	2	4	63.977	1.4541	9
-3	1	1	34.603	2.5901	33	-5	0	2	51.778	1.7642	3	2	2	4	64.039	1.4528	3
-3	1	2	34.657	2.5861	1	1	3	1	51.969	1.7581	1	-2	2	6	64.270	1.4481	5
2	0	2	35.585	2.5208	13	0	1	5	52.493	1.7418	2	-3	2	6	64.845	1.4367	7
-1	0	4	35.812	2.5053	5	-4	2	2	52.550	1.7401	2	4	0	3	65.927	1.4157	1
-1	2	2	36.592	2.4537	11	-2	3	1	52.968	1.7273	3	0	4	0	66.391	1.4069	21
-3	1	3	37.464	2.3986	27	-4	2	1	53.512	1.7110	1	2	1	5	66.740	1.4004	3
0	2	2	37.483	2.3974	24	-4	1	5	53.773	1.7033	5	-2	1	7	67.010	1.3954	2
-2	2	1	37.851	2.3749	4	2	0	4	54.011	1.6964	1	5	2	0	67.309	1.3899	2
2	1	2	39.124	2.3005	1	-2	0	6	54.267	1.6890	3	4	2	2	67.380	1.3887	14
-2	2	2	39.186	2.2971	11	-5	1	2	54.462	1.6834	2	-4	2	6	67.738	1.3822	1
1	1	3	39.219	2.2952	5	-5	1	3	54.526	1.6816	2	-6	1	1	68.685	1.3654	1
-2	1	4	39.320	2.2895	2	-3	0	6	54.905	1.6709	3	1	3	4	68.777	1.3638	2
-1	1	4	39.333	2.2888	2	-1	3	3	56.028	1.6400	11	-1	3	5	68.877	1.3621	1

a 8.856(1), b 5.6291(7), c 10.148(1) Å, β 115.516(6)°, V 456.58(9) Å^3

Table 2. Calculated powder X-ray diagram of synthetic piemontite crystallized from p = 0.75 starting material at 350 MPa and 500°C. All 2θ-values are given for CuKα

h	k	l	2θ	$d_{calc.}$	I/I_0	h	k	l	2θ	$d_{calc.}$	I/I_0	h	k	l	2θ	$d_{calc.}$	I/I_0
0	0	1	9.643	9.1644	2	-2	1	4	39.272	2.2922	3	4	2	0	56.344	1.6315	3
1	0	0	11.062	7.9915	4	-1	1	4	39.280	2.2917	2	-5	1	1	56.357	1.6312	11
-1	0	1	11.113	7.9549	1	-1	2	3	41.614	2.1685	5	-4	2	4	56.532	1.6265	16
-1	0	2	17.671	5.0150	23	-4	0	1	41.892	2.1547	14	-5	1	4	56.535	1.6265	1
0	1	1	18.423	4.8118	2	-4	0	3	42.010	2.1489	3	1	2	4	56.563	1.6258	7
1	1	0	19.214	4.6156	1	0	1	4	42.540	2.1234	2	2	1	4	56.577	1.6238	2
-1	1	1	19.244	4.6084	1	2	2	1	42.681	2.1167	17	2	3	1	56.666	1.6230	2
2	0	0	22.230	3.9957	13	-2	2	3	42.797	2.1112	16	3	2	2	57.043	1.6132	5
-2	0	2	22.333	3.9774	17	0	2	3	43.586	2.0748	14	0	3	3	57.403	1.6039	4
1	1	1	23.622	3.7633	5	2	0	3	44.376	2.0397	7	-4	0	6	58.060	1.5873	13
-1	1	2	23.695	3.7518	1	-3	2	1	44.600	2.0299	3	-3	3	1	58.237	1.5829	9
-2	1	1	25.533	3.4858	25	4	0	0	45.356	1.9979	6	1	1	5	58.582	1.5744	6
1	0	2	26.235	3.3940	11	-1	0	5	45.735	1.9822	1	5	1	0	60.109	1.5380	3
2	0	1	27.917	3.1933	10	-3	0	5	46.457	1.9531	1	4	1	2	60.172	1.5366	6
-2	0	3	28.084	3.1747	1	2	1	3	47.340	1.9186	3	-3	3	3	60.191	1.5361	5
0	0	3	29.210	3.0548	4	2	2	2	48.330	1.8816	9	0	0	6	60.571	1.5274	1
-3	0	1	30.626	2.9167	2	-2	2	4	48.488	1.8759	13	-4	2	5	61.306	1.5108	2
-3	0	2	30.684	2.9114	14	-1	2	4	48.495	1.8756	5	-5	2	1	63.728	1.4591	1
-1	1	3	30.762	2.9011	100	1	1	4	48.517	1.8748	4	-5	2	4	63.892	1.4558	9
0	2	0	31.624	2.8270	35	-1	1	5	48.635	1.8706	4	-6	0	4	63.897	1.4557	5
2	1	1	32.166	2.7805	10	3	1	2	49.051	1.8556	3	2	2	4	63.931	1.4550	3
-2	1	3	32.314	2.7681	1	1	3	0	49.661	1.8343	1	3	0	4	63.947	1.4547	2
0	1	3	33.310	2.6876	27	3	2	1	51.077	1.7867	1	-2	2	6	64.450	1.4506	5
1	2	0	33.599	2.6651	21	0	2	4	51.286	1.7799	3	-3	2	6	64.731	1.4389	6
3	0	0	33.616	2.6638	15	-5	0	2	51.791	1.7637	4	4	0	3	65.918	1.4159	1
-3	1	1	34.574	2.5921	38	0	1	5	52.436	1.7436	2	0	4	0	66.044	1.4135	22
-3	1	2	34.626	2.5884	1	-4	2	2	52.457	1.7429	2	-6	1	4	66.242	1.4197	1
2	0	2	35.578	2.5213	15	-2	3	1	52.746	1.7340	3	-3	1	7	66.645	1.4022	1
-1	0	4	35.788	2.5069	3	-4	1	5	53.736	1.7044	6	2	1	5	66.688	1.4014	4
-1	2	2	36.455	2.4626	10	2	0	4	53.989	1.6970	1	-2	1	7	66.944	1.3966	1
0	2	2	37.346	2.4059	24	-2	0	6	54.231	1.6900	3	5	2	0	67.234	1.3913	3
-3	1	3	37.429	2.4007	28	-5	1	2	54.450	1.6837	2	4	2	2	67.292	1.3902	15
-2	2	1	37.724	2.3826	4	-5	1	3	54.511	1.6820	2	-4	2	6	67.633	1.3741	1
-2	2	2	39.059	2.3042	11	-3	0	6	54.875	1.6717	3	1	3	4	68.567	1.3675	2
2	1	2	39.086	2.3027	2	-1	3	3	55.804	1.6460	11	-1	3	5	68.662	1.3658	1
1	1	3	39.172	2.2979	5	1	0	5	56.055	1.6393	1	-6	1	1	68.680	1.3655	1
-3	0	4	39.268	2.2924	1	-1	0	6	56.185	1.6358	11	0	2	6	69.949	1.3438	3

a 8.8548(8), b 5.6541(9), c 10.1546(9) Å, β 115.514(6)°, V 458.82(7) Å^3

Table 3. Calculated powder X-ray diagram of synthetic piemontite crystallized from p = 1.0 starting material at 350 MPa and 500°C. All 2θ-values are given for CuKα

h	k	l	2θ	$d_{calc.}$	I/I_0	h	k	l	2θ	$d_{calc.}$	I/I_0	h	k	l	2θ	$d_{calc.}$	I/I_0
0	0	1	9.644	9.1630	2	-3	0	4	39.288	2.2913	2	-4	2	4	56.499	1.6274	17
1	0	0	11.069	7.9869	5	-1	2	3	41.545	2.1719	6	1	2	4	56.511	1.6271	7
-1	0	1	11.120	7.9500	3	-4	0	1	41.921	2.1533	15	2	3	1	56.542	1.6263	2
-1	0	2	17.677	5.0133	26	-4	0	3	42.039	2.1475	2	-5	1	4	56.558	1.6259	1
1	1	0	19.181	4.6234	2	0	1	4	42.527	2.1240	1	2	1	4	56.573	1.6255	2
-1	1	1	19.211	4.6162	4	2	2	1	42.618	2.1197	18	-2	1	6	56.810	1.6192	1
2	0	0	22.242	3.9935	14	-2	2	3	42.735	2.1142	18	3	2	2	57.000	1.6143	5
-2	0	2	22.347	3.9750	20	0	2	3	43.518	2.0779	14	0	3	3	57.276	1.6072	5
1	1	1	23.596	3.7674	4	2	0	3	44.387	2.0392	7	-4	0	6	58.088	1.5866	12
-1	1	2	23.670	3.7558	2	-3	2	1	44.547	2.0323	3	-3	3	1	58.122	1.5858	10
-2	1	1	25.516	3.4881	29	4	0	0	45.383	1.9967	6	-3	3	2	58.157	1.5849	1
1	0	2	26.241	3.3934	12	-1	0	5	45.743	1.9818	1	1	1	5	58.576	1.5746	5
2	0	1	27.928	3.1921	11	-3	0	5	46.476	1.9523	1	-3	3	3	60.079	1.5387	5
0	0	3	29.214	3.0544	4	2	1	3	47.334	1.9189	4	5	1	0	60.130	1.5375	3
-3	0	1	30.647	2.9148	1	2	2	2	48.274	1.8837	9	4	1	2	60.183	1.5363	7
1	1	2	30.680	2.9117	2	-2	2	4	48.433	1.8779	11	0	0	6	60.580	1.5272	1
-3	0	2	30.705	2.9094	14	-1	2	4	48.436	1.8778	6	-4	2	5	61.276	1.5115	2
-1	1	3	30.777	2.9028	100	1	1	4	48.508	1.8752	5	-6	0	3	62.974	1.4748	1
0	2	0	31.532	2.8350	38	-1	1	5	48.627	1.8709	2	-5	0	6	63.580	1.4622	1
2	1	1	32.153	2.7816	8	3	1	2	49.052	1.8556	3	-5	2	1	63.707	1.4596	1
-2	3	1	32.302	2.7691	3	1	3	0	49.520	1.8392	2	-5	2	4	63.873	1.4562	10
0	1	3	33.291	2.6890	29	3	2	1	51.030	1.7883	1	2	2	4	63.888	1.4559	4
1	2	0	33.514	2.6717	22	0	2	4	51.228	1.7818	3	-6	0	4	63.946	1.4547	4
3	0	0	33.635	2.6623	16	1	3	1	51.604	1.7697	1	3	0	4	63.964	1.4543	2
-3	1	1	34.572	2.5923	40	-5	0	2	51.892	1.7625	4	-2	2	6	64.108	1.4514	4
-3	1	2	34.624	2.5885	2	-4	2	2	52.421	1.7440	2	-3	2	6	64.696	1.4396	7
2	0	2	35.588	2.5206	16	0	1	5	52.428	1.7438	2	0	4	0	65.832	1.4175	22
-1	0	4	35.796	2.5065	3	-2	3	1	52.615	1.7381	4	4	0	3	65.943	1.4154	1
-1	2	2	36.376	2.4677	10	-4	1	5	53.749	1.7040	6	-3	1	7	66.652	1.4020	1
0	2	2	37.267	2.4108	24	-2	0	6	54.245	1.6896	3	2	1	5	66.687	1.4014	4
-3	1	3	37.429	2.4007	31	-5	1	2	54.472	1.6831	2	-2	1	7	66.946	1.3966	1
-2	2	1	37.653	2.3870	4	-5	1	3	54.533	1.6814	2	5	2	0	67.214	1.3917	3
2	2	0	38.927	2.3117	1	-3	0	6	54.895	1.6711	3	4	2	2	67.263	1.3908	14
-2	2	2	38.991	2.3081	11	-1	3	3	55.676	1.6495	11	-4	2	6	67.607	1.3845	1
2	1	2	39.086	2.3032	2	1	0	5	56.064	1.6390	1	1	3	4	68.456	1.3694	2
1	1	3	39.158	2.2986	7	-1	0	6	56.195	1.6355	11	-6	1	1	68.714	1.3649	1
-2	1	4	39.265	2.2926	4	4	2	0	56.309	1.6325	3	0	2	6	69.906	1.3445	3
-1	1	4	39.268	2.2925	2	-5	1	1	56.379	1.6306	11						

a 8.8490(9), *b* 5.6670(4), *c* 10.153(1) Å, β 115.499(6)°, *V* 459.75(7) Å^3

Table 4. Calculated powder X-ray diagram of synthetic piemontite crystallized from p = 1.25 starting material at 350 MPa and 500°C. All 2θ-values are given for CuKα

h	k	l	2θ	$d_{calc.}$	I/I_0	h	k	l	2θ	$d_{calc.}$	I/I_0	h	k	l	2θ	$d_{calc.}$	I/I_0
0	0	1	9.607	9.1991	4	-3	0	4	39.162	2.2984	3	-5	1	4	56.389	1.6303	2
1	0	0	11.050	8.0005	4	-1	2	3	41.364	2.1824	7	2	1	4	56.404	1.6299	2
-1	0	1	11.090	7.9719	3	-4	0	1	41.843	2.1571	20	-2	1	6	56.587	1.6251	1
-1	0	2	17.617	5.0303	28	-4	0	3	41.934	2.1526	3	3	2	2	56.800	1.6195	7
1	1	0	19.095	4.6441	2	0	1	4	42.372	2.1314	2	0	3	3	56.958	1.6154	5
-1	1	1	19.118	4.6385	4	2	2	1	42.435	2.1284	17	-3	3	1	57.825	1.5932	11
2	0	0	22.204	4.0003	12	-2	2	3	42.525	2.1241	19	-4	0	6	57.885	1.5917	13
-2	0	2	22.285	3.9860	20	0	2	3	43.309	2.0874	14	1	1	5	58.381	1.5794	5
1	1	1	23.506	3.7816	4	2	0	3	44.278	2.0440	8	-1	1	6	58.479	1.5770	1
-2	1	1	25.426	3.5002	33	-3	2	1	44.364	2.0402	3	-3	3	3	59.761	1.5462	5
1	0	2	26.175	3.4018	15	4	0	0	45.302	2.0001	5	5	1	0	59.998	1.5406	2
2	1	0	27.207	3.2750	2	2	1	3	47.197	1.9241	5	4	1	2	60.039	1.5397	9
2	0	1	27.875	3.1983	7	2	2	2	48.081	1.8908	9	0	0	6	60.373	1.5319	1
0	0	3	29.122	3.0639	5	-2	2	4	48.204	1.8863	11	-4	2	5	61.017	1.5173	2
1	1	2	30.574	2.9215	4	-1	2	4	48.206	1.8862	7	-5	0	6	63.369	1.4665	1
-3	0	1	30.589	2.9215	4	1	1	4	48.349	1.8810	5	-5	2	1	63.506	1.4637	2
-3	0	2	30.634	2.9160	17	-1	1	5	48.441	1.8776	4	-5	2	4	63.631	1.4611	11
-1	1	3	30.649	2.9146	100	3	1	2	48.928	1.8600	1	2	2	4	63.648	1.4608	4
0	2	0	31.343	2.8516	37	1	3	0	49.222	1.8496	2	-6	0	4	63.784	1.4580	5
2	1	1	32.060	2.7894	9	3	2	1	50.844	1.7944	1	3	0	4	63.803	1.4576	2
-2	1	3	32.175	2.7797	2	0	2	4	50.999	1.7893	3	-2	2	6	63.818	1.4573	5
0	1	3	33.164	2.6991	31	-5	0	2	51.723	1.7659	5	-3	2	6	64.406	1.4454	8
1	2	0	33.329	2.6861	26	-4	2	2	52.225	1.7501	2	5	1	1	65.391	1.4260	1
3	0	0	33.577	2.6668	17	0	1	5	52.239	1.7497	2	0	4	0	65.399	1.4258	24
-3	1	1	34.477	2.5993	43	-2	3	1	52.318	1.7472	4	4	0	3	65.795	1.4182	1
-3	1	2	34.517	2.5963	1	-4	2	1	53.198	1.7204	1	-6	1	4	66.092	1.4126	2
2	0	2	35.510	2.5259	19	-4	1	5	53.559	1.7096	5	-3	1	7	66.385	1.4070	1
-1	0	4	35.671	2.5149	2	-5	0	1	53.559	1.7096	5	2	1	5	66.479	1.4053	5
-1	2	2	36.179	2.4808	9	-2	0	6	54.045	1.6954	4	-2	1	7	66.678	1.4016	1
0	2	2	37.071	2.4231	27	-5	1	3	54.387	1.6855	2	5	2	0	67.009	1.3954	3
-3	1	3	37.301	2.4087	33	-3	0	6	54.695	1.6768	4	4	2	2	67.048	1.3947	16
-2	2	1	37.468	2.3983	4	-1	3	3	55.358	1.6582	11	2	3	3	67.197	1.3954	2
2	2	0	38.747	2.3220	2	-1	0	6	55.993	1.6409	13	1	3	4	68.115	1.6375	2
-2	2	2	38.796	2.3192	13	4	2	0	56.121	1.6375	4	-1	3	5	68.189	1.3741	1
2	1	2	38.965	2.3095	3	2	3	1	56.246	1.6342	2	-4	1	7	68.396	1.3705	2
1	1	3	39.029	2.3059	6	-5	1	1	56.251	1.6340	10	-6	1	1	68.560	1.3676	1
-2	1	4	39.111	2.3013	6	-4	2	4	56.268	1.6336	20	0	2	6	69.609	1.3495	4
-1	1	4	39.114	2.3011	1	1	2	4	56.279	1.6333	8						

a 8.8625(7), *b* 5.7006(3), *c* 10.1822(9) Å, β 115.525(6)°, *V* 464.21(6) Å^3

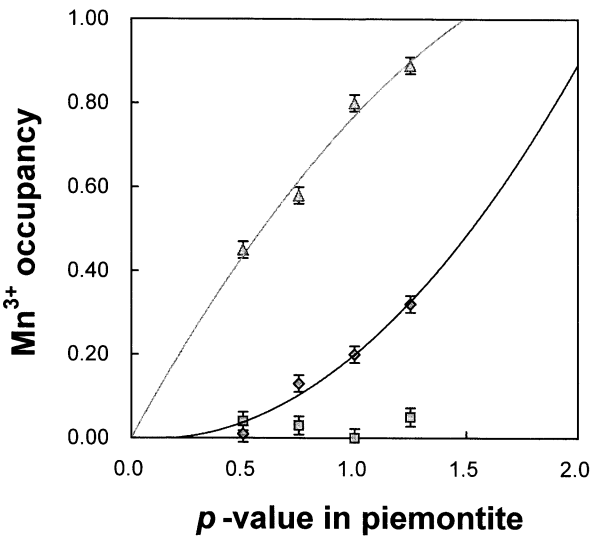

Fig. 3. Variation of the cation site occupancies of the *M1*, *M2* and *M3* sites in piemontite as a function of *p*-value. Filled triangles, filled diamonds and filled squares represent Mn^{3+}-occupancies of the *M3*, *M1* and *M2* sites from this study, respectively. Error bars represent one standard deviation.

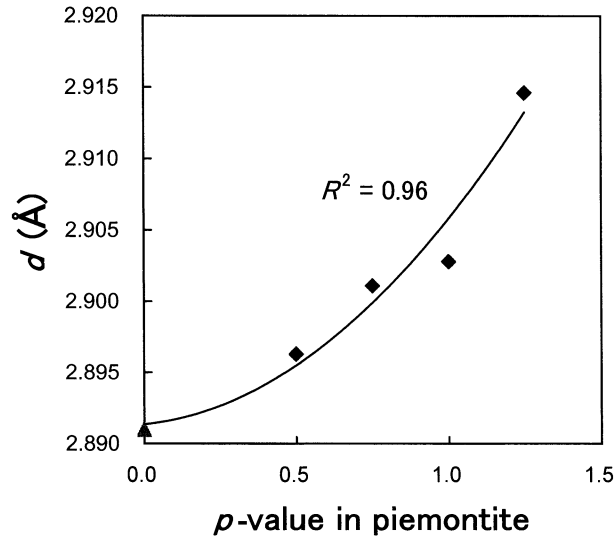

Fig. 4. Variation of the *d*-values of the strongest line in the simulated powder patterns of piemontite as a function of *p*-value. Filled diamonds are the *d*-values of synthetic piemontites from this study. The filled triangleis clinozoisite calculated using the refined structural parameters of Dollase (1968).

with profile relaxation or the Pearson VII function in RIETAN-2000. An asymmetric parameter is built into this profile function. Details of these profile functions are given by Izumi and Ikeda (2000). Nonlinear least-squares calculation using Marquardt method was followed by the conjugate-direction method to check convergence at local minima (Izumi, 1993). Preferred orientation was corrected using the March-Dollase function (Dollase, 1986).

The Rietan-2000 program has a function which allows simulation of ideal powder patterns. The simulation is not affected by preferred orientation, and thus was carried out using the obtained unit-cell parameters, site occupancies, atomic positions and structural parameters.

Results

Simulated powder diffraction patterns of synthetic piemontites with p = 0.5, 0.75, 1.0 and 1.25 are listed in Tables 1, 2, 3 and 4, respectively, where peaks having intensities less than one percent of the strongest peak are ignored. The refined unit-cell parameters are also listed in Tables 1, 2, 3 and 4. A complete chart of the powder diffraction pattern calculated for p = 1.0 piemontite is given in Fig. 1. Variations of the unit-cell parameters against p-value of synthesized piemontite show similar trends to those of Anastasiou and Langer (1977) (Fig. 2).

Discussion

The powder pattern of p = 1.0 piemontite from this study can be compared directly with that by Anastasiou and Langer (1977). We found two apparent errors in their indexing: the 133 ($d_{calc.}$ = 2.906 Å) and 326 ($d_{calc.}$ = 1.441 Å) peaks in Anastasiou and Langer (1977) should be $\bar{1}13$ and $\bar{3}26$, respectively, as shown in Table 3. Although Anastasiou and Langer (1977) assigned the peak $\bar{4}02$ ($d_{calc.}$ = 2.146 Å), the calculated intensity in our present study is too low to be adopted. On the basis of our calculations, the $\bar{3}22$ ($d_{calc.}$ = 2.028 Å) and $\bar{6}02$ ($d_{calc.}$ = 1.455 Å) peaks in Anastasiou and Langer (1977) are not sufficiently intense to be observed for p = 1.0 piemontite. However, the $\bar{3}22$ peak was observed in the calculated powder pattern of p = 0.5 piemontite (Table 1).

Anastasiou and Langer (1977) suggested that the wide spread variation of unit-cell parameters in natural piemontite was caused by cations other than Ca occupying the *A2* site, or other than Al and Mn at the octahedral sites. However, we consider that misindexing of the Miller indices for each reflection may also be a possible cause of the variable cell parameters.

The variations of the unit-cell parameters as a function of p-value in our piemontites are similar to those of Anastasiou and Langer (1977). The a-axis decreases with increasing p up to near p = 1, and subsequently increases at p>1 (Fig. 2). In contrast, the c-dimension does not change significantly from p = 0.0 to about p = 0.75, but then increases steeply above p = 0.75. Anastasiou and Langer (1977) interpreted the breaks in the cell parameters vs. composition near p = 1.0 as due to predominant entrance of Mn^{3+} into *M3* below p = 1.0 and into *M1* above p = 1.0. However, our results do not necessarily support this interpretation. Firstly, in our study there seems no break between each cell dimensions near p = 1. Secondly, the interpretation of the 'break' of cell parameters by Anastasiou and Langer (1977) does not seem reasonable, because Mn^{3+} enters the *M1* site even if the *M3* site is not

filled by Mn^{3+} (Fig. 3), and thus the change in cell dimensions must be gradual. Moreover, with increasing Mn^{3+} occupancies in the *M3* and *M1* sites, the *M3* and *M1* octahedra are distorted to form tetragonally compressed octahedral, which also causes gradual nonlinear variation of cell parameters. The *d*-values of the strongest line in the simulated powder patterns shows comparable variation with the unit-cell parameters (Fig. 4). Variation is nonlinear (d (Å) = $0.012p^2 + 0.002p + 2.891$; $R^2 = 0.958$) when clinozoisite data ($d_{calc.} = 2.891$ Å at $p = 0$) calculated by using the refined structural parameters of Dollase (1968) is included.

Calculated powder patterns of Cz–Pm synthetic piemontites have not been published to date. From the simulation of X-ray powder diffraction patterns, we have clearly identified systematic variations in *d*-value. These patterns are very useful for indexing each reflection in X-ray powder diffraction patterns of natural piemontite, and in avoiding misindexing and miscalculation of unit-cell parameters. Moreover, by comparison with these simulated X-ray powder patterns, we can evaluate the effects of preferred orientation in measured X-ray powder diffraction patterns. This is important for X-ray powder crystal structure analysis.

Acknowledgements

Our thanks to Dr. Fujio Izumi of National Institute for his permission to use the Rietan-2000 program and for his help; and to Dr. Barry Roser of Shimane University for his critical reading of the manuscript.

References

Albee, A.L., and Chodos, A.A. (1970) Semiquantitative electron microprobe determination of Fe^{2+}/Fe^{3+} and petrologic problems. *American Mineralogist*, **55**, 491-501.

Anastasiou, P., and Langer, K. (1977) Synthesis and physical properties of piemontite $Ca_2Al_{3-p}Mn^{3+}{}_p(Si_2O_7/SiO_4/O/OH)$. *Contributions to Mineralogy and Petrology*, **60**, 225-245.

Bish, D.L., and Reynolds, R.C. (1989) Sample preparation for X-ray diffraction. In: Bish, D.L., and Post, J.E. (eds.) "*Reviews in Mineralogy Vol 20, Modern powder diffraction*", pp 73-99. Mineralogical Society of America, Washington, DC.

Bonazzi, P., and Menchetti, S. (1994) Structural variations induced by heat treatment in allanite and REE-bearing piemontite. *American Mineralogist*, **79**, 1176-1184.

Bonazzi, P., and Menchetti, S. (1995) Monoclinic members of the epidote group: effects of the $Al \rightleftarrows Fe^{3+} \rightleftarrows Fe^{2+}$ substitution and of the entry of REE^{3+}. *Mineralogy and Petrology*, **53**, 133-153.

Bonazzi, P., Menchetti, S., and Palenzona, A. (1990) Strontiopiemontite, a new member of the epidote group from Val Graveglia, Liguria, Italy. *European Journal of Mineralogy*, **2**, 519-523.

Bonazzi, P., Garbarino, C., and Menchetti, S. (1992) Crystal chemistry of piemontites: REE-bearing piemontite from Monte Brugiana, Alpi Apuane, Italy. *European Journal of Mineralogy*, **4**, 23-33.

Dollase, W.A. (1968) Refinement and comparison of the structures of zoisite and clinozoisite. *American Mineralogist*, **53**, 1882-1898.

Dollase, W.A. (1969) Crystal structure and cation ordering of piemontite. *American Mineralogist*, **54**, 710-717.

Dollase, W.A. (1971) Refinement of the crystal structures of epidote, allanite and hancockite. *American Mineralogist*, **56**, 447-464.

Dollase, W.A. (1986) Correction of intensities for preferred orientation in powder diffractometry: application of the March model. *Journal of Applied Crystallography*, **19**, 267-272.

Ferraris, G., Ivaldi, G., Fuess, H., and Gregson, D. (1989) Manganese/iron distribution in a strontian piemontite by neutron diffraction. *Zeitschrift für Kristallographie*, **187**, 145-151.

Izumi, F. (1993) Rietveld analysis program RIETAN and PREMOS and special applications. In: Young RA (ed.) "*the Rietveld Method*", pp 236-253. Oxford Science Publications

Izumi, F., and Ikeda, T. (2000) A Rietveld analysis program RIETAN?98 and its application to zeolites. *Material Science Forum*, 321-324.

Kimura, Y., and Akasaka, M. (1999) Estimation of Fe^{2+}/Fe^{3+} and Mn^{2+}/Mn^{3+} ratios by electron probe micro analyzer. *Journal of the Mineralogical Society of Japan*, **28**, 159-166 (in Japanese).

Kvick, A., Pluth, J.J., Richardson, J.W., and Smith, J.V. (1988) The ferric ion distribution and hydrogen bonding in epidote: a neutron diffraction study at 15 K. *Acta Crystallographica*, **B 44**, 351-355.

Langer, K., Tillmanns, E., Kersten, M., Almen, H., and Arni, R.K. (2002) The crystal chemistry of Mn^{3+} in the clino- and orthozoisite structure types, $Ca_2M^{3+}{}_3$ [OH/O/SiO_4/Si_2O_7] : A structural and spectroscopic study of some natural piemontites and "thulites" and their synthetic equivalents. *Zeitschrift für Kristallographie* **217**, 1-18.

Nagashima and Akasaka (2004) An X-ray Rietveld study of piemontite on the join $Ca_2Al_3Si_3O_{12}(OH) - Ca_2Mn^{3+}{}_3Si_3O_{12}(OH)$ formed by hydrothermal synthesis. American Mineralogist (in press)

Post, J.E., and Bish, D.L. (1989) In: Bish DL, Post JE (eds.) Rietveld refinement of crystal structures using powder X-ray diffraction data. "*Reviews in Mineralogy Vol 20, Modern powder diffraction*", pp 277-308. Mineralogical Society of America, Washington, DC

Toraya, H. (1990) Array-type universal profile function for powder pattern fitting. *Journal of Applied Crystallography*, **23**, 485-491.

(Received: Nov. 21, 2003, Accepted: Dec. 12, 2003)

（要　旨）

永嶌真理子・赤坂正秀，2003，$Ca_2Al_3Si_3O_{12}(OH)$–$Ca_2Mn^{3+}{}_3Si_3O_{12}(OH)$系合成紅簾石におけるX線回折パターンのシミュレーション，島根大学地球資源環境学研究報告，22，159-164

$Ca_2Al_3Si_3O_{12}(OH)$–$Ca_2Mn^{3+}{}_3Si_3O_{12}(OH)$系紅簾石を合成し，理想的なX線粉末回折パターンのシミュレーションを行った．シミュレーションは，リートヴェルト解析によって得られた格子定数・席占有率・原子座標などの構造パラメータを用い，Rietan-2000プログラムで行われた．合成$Ca_2Al_{3-p}Mn^{3+}{}_pSi_3O_{12}(OH)$–紅簾石の組成は，$p$ = 0.5，0.75，1.0，1.25である．シミュレーションされた粉末回折パターンにおける最強線の面間隔dの値は非直線的な変化を示しており，この変化は格子定数変化と対応している．シミュレーションされたパターンは，天然紅簾石のX線粉末回折パターンにミラー指数を付ける際に誤った指数を付けたり，それによって計算される格子定数の間違いを避けるのに非常に有用である．さらにシミュレーションされたパターンと実測した粉末回折パターンを比較することにより，実際に測定されたパターンにおける選向配列の程度を評価することができる．このことはX線結晶構造解析を行う際に最も重要なことのひとつである．